

Improvement of the LbCas12a-crRNA system for efficient gene targeting in plants

Tien Van Vu (✉ tienvu.agi@gmail.com)

Division of Applied Life Science (BK21 FOUR Program), Plant Molecular Biology and Biotechnology Research Center, Gyeongsang National University <https://orcid.org/0000-0002-6369-7664>

Duong Thi Hai Doan

Division of Applied Life Science (BK21 FOUR Program), Plant Molecular Biology and Biotechnology Research Center, Gyeongsang National University

Mil Thi Tran

Division of Applied Life Science (BK21 FOUR Program), Plant Molecular Biology and Biotechnology Research Center, Gyeongsang National University

Yeon Woo Sung

Division of Applied Life Science (BK21 FOUR Program), Plant Molecular Biology and Biotechnology Research Center, Gyeongsang National University

Young Jong Song

Division of Applied Life Science (BK21 FOUR Program), Plant Molecular Biology and Biotechnology Research Center, Gyeongsang National University

Jae-Yean Kim (✉ kimjy@gnu.ac.kr)

Division of Applied Life Science (BK21 FOUR Program), Plant Molecular Biology and Biotechnology Research Center, Gyeongsang National University <https://orcid.org/0000-0002-1180-6232>

Research Article

Keywords: LbCas12a, Gene targeting, Gene editing, Homology-directed repair, SpCas9, geminiviral replicon

Posted Date: April 26th, 2021

DOI: <https://doi.org/10.21203/rs.3.rs-301508/v2>

License:   This work is licensed under a Creative Commons Attribution 4.0 International License.

[Read Full License](#)

Version of Record: A version of this preprint was published at Frontiers in Plant Science on August 10th, 2021. See the published version at <https://doi.org/10.3389/fpls.2021.722552>.

Abstract

Plant gene targeting (GT) can be utilized to precisely replace up to several kilobases of a plant genome. Recent studies using the powerful clustered regularly interspaced short palindromic repeats (CRISPR) and CRISPR-associated (Cas) nucleases significantly improved plant GT efficiency. However, GT for loci without associated selection markers is still inefficient. We previously utilized *Lachnospiraceae bacterium* Cas12a (LbCas12a) in combination with a replicon for tomato GT and obtained high GT efficiency with some selection markers. In this study, we optimize and advance our GT system by using a temperature-tolerant LbCas12a (ttLbCas12a) in combination with various crRNA forms and chemical treatments to suppress the canonical non-homologous end-joining pathway in tomato. Our work demonstrates the significance of the selection of gene scissors, the appropriate design and number of LbCas12a crRNAs, the use of chemical treatments, and the establishment of favorable experimental conditions for further enhancement of plant HDR to enable efficient GT in tomato.

Introduction

Plant gene targeting (GT) was first reported in 1988 by Paszkowski and coworkers, although that study only obtained low efficiency of targeting (Paszkowski et al., 1988), and GT usually requires at least one associated selection marker for the practical achievement of GT events (Puchta and Hohn, 2005; Van Vu et al., 2019). Without any targeted DSB and with an antibiotic selection marker, the GT efficiency remained extremely low (Terada et al., 2002). An important improvement was made to plant GT by introducing DSBs at the targeted sites using a pre-inserted I-SceI recognition sequence; this approach ultimately enhanced the GT efficiency up to hundreds of fold (Puchta et al., 1993; Puchta et al., 1996), but the efficiency was still low (i.e., up to 1.83%) even it required two selection markers. The subsequent development of the first, second and, especially, third generations of site-directed nucleases (SDNs) has revolutionized precision gene-editing technology with the easy customization of targeted DSBs at any site of interest for exchanging donor DNA templates (Shan et al., 2013; Wright et al., 2005; Zhang et al., 2013).

Until recently, SDN-based GT efficiency has been significantly enhanced through combinations of SDN complexes and geminiviral replicons, which are autonomously replicative vectors for supplying high doses of homologous DNA template to DSB repair foci (Butler et al., 2016; Cermak et al., 2015; Gil-Humanes et al., 2017; Vu et al., 2020). Further improvement of plant GT was also possible with the suppression of cNHEJ (Endo et al., 2016; Maruyama et al., 2015; Qi et al., 2013; Robert et al., 2015) or activation of HDR mechanisms (Song et al., 2016) using biological approaches or chemical treatments. Nevertheless, chemical treatments have not been heavily studied in conjunction with CRISPR/Cas-based GT in plants. Overall, the practical GT efficiency with allele-associated selection markers was approximately 10% in most of the “accessible” plants and considerably lower in difficult systems or those with targeted loci lacking selection markers (Van Vu et al., 2019). Therefore, continuous improvement of plant GT remains necessary, especially for applications in less accessible plants.

Our previous work showed the significant improvement of plant GT using geminiviral replicons and LbCas12a, rather than SpCas9 (Vu et al., 2020). More importantly, the activity of LbCas12a nucleases was more temperature-dependent than that of SpCas9 (Malzahn et al., 2019; Vu et al., 2020). Recently, a temperature-tolerant LbCas12a mutant (D156R), known as ttLbCas12a, which exhibited significantly improved cleavage activity and hence gene targeting efficiency, was reported in *Arabidopsis* using floral dipping-based gamete stage transformation (Merker et al., 2020a; Schindele and Puchta, 2020). However, further characterization of ttLbCas12a for somatic cell-based GT systems such as tomato GT, especially in combination with DNA replicons, has not been undertaken. We hypothesized that ttLbCas12a could be utilized to further improve our replicon-based plant GT system through appropriate customization of its nuclease-crRNA complexes. Chemical treatment for suppressing cNHEJ or activating HDR pathways was also tested and validated for practical GT applications in tomato. In this report, we describe a further comparison of LbCas12a and SpCas9 in inducing GT at the same specific SIANT1 locus. Subsequently, extensive characterization of ttLbCas12a in comparison with LbCas12a is shown at the SIANT1, SIHKT1;2, and SIEPSPS1 loci with or without allele-associated selection markers. Our work demonstrates the significance of utilizing the appropriate design of CRISPR/Cas-crRNA complexes, chemical treatments, and favorable experimental conditions to further enhance plant HDR for efficient GT in tomato.

Results

NU7441 treatment enhances LbCas12a-based GT efficiency

A plant genomic DNA DSB may be repaired by two major competing mechanisms, namely, cNHEJ and HDR. The GT approach is based on the HDR mechanism; therefore, to increase its efficacy, blocking the cNHEJ pathway is a good option (Van Vu et al., 2019). A number of studies have been published regarding the uses of chemical treatments for blocking cNHEJ to enhance GT efficiency in mammals (Chu et al., 2015; Maruyama et al., 2015; Robert et al., 2015; Zhang et al., 2017). However, only limited information regarding the applications of the chemicals to plant GT is currently available. Therefore, we selected SCR7 (an inhibitor of DNA ligase IV), NU7441 (a DNA-dependent protein kinase (DNA-PKcs) inhibitor), and KU0060648 (a dual inhibitor of DNA-PKcs and phosphatidylinositol-3 kinase (PI-3K)) to determine their effects on plant GT. Previously, a replicon-based CRISPR/Cas-mediated targeted DNA insertion system was successfully developed with SIANT1 as a visible marker (Cermak et al., 2015; Vu et al., 2020). We used SpCas9 (pTC217) and LbCas12a (pHR01 and pMR01) carrying GT vectors to assess the effects of chemical treatments and GT scoring followed Vu and coworkers (2020) since the scoring total GT callus number provides richer data than simply scoring GT cotyledon number.

During the GT reaction performed using the SpCas9-based pTC217 vector, treatment with the DNA ligase IV inhibitor led to an improvement in the GT efficiency compared to the mock control (Figure 1a, upper panel). The GT efficiency was increased to around 3.3% with the treatments of either 10 or 50 μ M SCR7 compared to the mock 0 μ M treatment or the 1 μ M SCR7 treatment (Supplemental Table 1). However, Fisher's LSD test for comparison of the GT efficiency between the treated concentrations and the mock

control did not return significant p-values to determine whether the GT enhancement was strong enough (Figure 1a, upper panel). The data indicate that 10 μ M SCR7 was the best concentration for SpCas9-based GT in tomato. By contrast, the LbCas12a-based pHR01 construct exhibits a decreasing trend from the mock control to the highest SCR7 concentration. There were mild GT efficiency changes among the mock and 1 or 10 μ M SCR7 treatments. Nevertheless, the GT efficiency was dramatically reduced to $4.140 \pm 0.66\%$ at 50 μ M SCR7 from $6.95 \pm 0.91\%$ in the mock treatment (68% reduction) (Figure 1a, bottom panel; Supplemental Table 1).

To test the impacts of NU7441 and KU0060648 on CRISPR/Cas-based GT in tomato, we employed both single and multiple replicon systems to carry the SpCas9 or LbCas12a constructs. In the case of SpCas9, the GT efficiency was slightly increased (Figure 1b, top panel) when 0.2 μ M KU0060648 or 1 μ M NU7441, which were within the optimal concentration ranges tested in human cells (Robert et al., 2015), was applied to NSEL medium (Supplemental Figure 1) and incubated from days 3 to 8 post-transformation. However, pairwise comparison resulted in p-values that were not small enough to reject the null hypothesis. A similar situation also occurred for the LbCas12a-based single replicon, although NU7441 treatment led to a smaller p-value. In this case, 1 μ M NU7441 treatment resulted in GT efficiency at $11.07 \pm 1.50\%$ compared to $7.17 \pm 1.67\%$ of that of the mock control, which represented a 1.54-fold enhancement (Figure 1b, middle panel, Supplemental Table 2). The effect is considerably more clear with NU7441 treatment using the LbCas12a-based multiple replicon system. Blocking cNHEJ with 1 μ M NU7441 significantly increased the multireplicon-based GT efficiency from $11.01 \pm 0.93\%$ in the mock control to $15.89 \pm 1.15\%$, representing an approximately 1.44-fold change (Figure 1b, bottom panel, Supplemental Table 2). There was almost no GT efficiency change in the case of KU0060648 treatment with pMR01.

Silver nitrate treatment enhances GT efficiency and purple shoot regeneration

Recently, polyamines, such as putrescine, spermidine, and spermine, were shown to enhance HDR by facilitating RAD51-mediated homologous strand annealing and synaptic complex formation in mice (Lee et al., 2019). We added 1 mM putrescine, spermidine, or spermine to the NSEL medium and incubated the transformed explants for 5 days after cocultivation with agrobacteria carrying the pMR01 plasmid. In contrast to the observations made in animals, no improvement in GT efficiency was achieved by any of the polyamines in the two replicates (Supplemental Table 3). In fact, the GT efficiency was reduced with supplementation with longer chain polyamines (i.e., spermidine and spermine) (Supplemental Figure 2). We also observed a higher proliferation of the purple GT calli and a delay in shoot formation from the explants treated with spermidine or spermine compared to the mock control. We surmised that direct supplementation with synthetic polyamines, especially spermidine and spermine, at high concentrations might not facilitate organ regeneration. Thus, we next used silver nitrate (AgNO_3) to increase endogenous polyamines. Silver nitrate was shown to stimulate the activity of arginine decarboxylase (ADC; EC 4.1.1.9), one of the key enzymes of putrescine and polyamine biosynthesis (Hanfrey et al., 2001). Using

the pMR01 vector for this experiment, we treated the transformed explants with 30 μM AgNO_3 for 5 days on NSEL medium. In two replicates, we observed a significant increase in the number of purple GT spots per explant compared to that of the mock control at 21-day post-transformation (dpt) (Supplemental Figure 3a; Supplemental Table 4). Furthermore, the addition of AgNO_3 at a later stage, in the first subculture with the SEL4C medium, stimulated shoot regeneration from purple calli (Supplemental Figure 3b). This finding is consistent with that silver nitrate enhances somatic embryogenesis (Beyer, 1976; Giridhar et al., 2004; Roustan et al., 1990).

LbCas12a-based GT is superior to the SpCas9-based GT

In our previous report, LbCas12a was shown to mediate GT more effectively than the SpCas9 system. The comparisons were conducted at the SIANT1 locus under various experimental conditions (Vu et al., 2020). However, the comparison using the replicon-based pTC217 and pHR01 constructs might have flawed parameters, such as slightly different SSN-mediated binding and cutting sites and donors. Furthermore, the promoter and terminator driving the expression of SpCas9 and LbCas12a might also contribute to the differences. To better characterize and compare the GT performance of SpCas9 and LbCas12a, we designed a GT system with specific SIANT1 cutting sites that are accessible to both nucleases (Figure 2a and Supplemental Figure 4) and the same promoter and terminator to drive the transcription of Cas nucleases. The comparisons were conducted using single sgRNAs (sgR2^{ANT1} vs. crR1.23^{ANT1} and crR3.20^{ANT1}, sgR3^{ANT1} vs. crR3.23^{ANT1}) (Figure 2b and Supplemental Data S1 file). The 20-nt cRNA was also used for the LbCas12a (crR3.20^{ANT1}) to mimic the exact binding sequences of the SpCas9 gRNAs (Supplemental Figure 4). Each of the GT tools was expressed from both the replicon and T-DNA to compare the GT efficiency of the two delivery methods (Figure 2b). Our data demonstrate the superiority of the replicon system compared to the T-DNA in plant GT, as the GT efficiencies were enhanced 5-8-fold with the replicons compared to that of the T-DNA tools (Figure 2c and Supplemental Figure 5).

Moreover, in keeping with our previous data (Vu et al., 2020), all of the LbCas12a-based GT constructs, except the 20-nt crRNA, exhibited significantly higher GT efficiencies than the SpCas9-based GT tools (Figure 2c, $8.00 \pm 1.11\%$ of pHRC01 vs. $5.1 \pm 0.35\%$ of pHRC04, $9.53 \pm 0.63\%$ of pHRC03 vs. $6.73 \pm 0.52\%$ of pHRC05). These results also indicate that the 23-nt crRNA LbCas12a mediated GT more effectively than the 20-nt crRNA (pHRC03 vs. pHRC02). Surprisingly, analysis of the indel mutation efficiency of the guide RNAs at the plant stage demonstrated a reverse correlation between the indel mutation efficiency and the GT efficiency at cutting site 1 and cutting site 2 (Figure 2d, pHRC01 vs. pHRC04 and pHRC03 vs. pHRC05, Supplemental Figure 5). This result indicates that a considerably stronger indel mutation activity may negatively affect the GT reactions. Since cNHEJ-mediated indel mutations are favored throughout the life cycle of the cells and HDR is limited to the S-G2 phases (Van Vu et al., 2019), DNA DSBs that form at cell cycles other than S-G2 may lead to permanent modifications at the cutting sites, resulting in the inhibition of any further cleavage at these sites in the HDR-favorable cell cycles. Our data confirmed the stronger activity of SpCas9 in generating DNA DSBs compared to that of LbCas12a in tomato. The

highest indel mutation rate was 49.5% on average with sgR2^{ANT1} (Supplemental Figure 5). Most of the mutation traces appear to be deletions (Supplemental Figure 6). In the experiment, we obtained GT events with a typical purple phenotype due to the overexpression of SIANT1 and the subsequent accumulation of anthocyanin in the plants (Supplemental Figure 7)

ttLbCas12a-based GT efficiency might be better than that of the wild-type variant in the case of the dual crRNA system.

The cleavage activity of Cas nucleases was shown to be temperature-dependent, especially in the case of LbCas12a (Malzahn et al., 2019). Previously, we showed the temperature dependency of CRISPR/Cas-mediated GT in tomato (Vu et al., 2020). In that case, LbCas12a exhibited considerably better GT support at temperatures as high as 31 °C compared to that at 19 °C or 25 °C. This result partially explained why SpCas9 was superior in indel mutation formation compared to LbCas12a at RT. Recently, Puchta's group reported a temperature-tolerant LbCas12a variant that significantly enhanced indel mutation (Schindele and Puchta, 2020) and GT (Huang et al., 2021; Merker et al., 2020a) efficacy in plants. The group used 24-nt single crRNAs that were released by ribozyme flanking sequences. It is interesting to characterize and compare the ttLbCas12a nuclease using our replicon system and on somatic cells of tomato. Here, we used a multiplexed editing approach with a single array of crRNAs and the gRNA length may affect the processing activity of the LbCas12a (Zetsche et al., 2017). We investigated the impacts of single and dual cleavages using 20- or 23-nt crRNA on the GT performance of both the wild-type and ttLbCas12a variants at the well-characterized SIANT1 locus (Figure 3a; Supplemental Figure 4 and Data S1 file). To contribute to the comparison data, another dual crRNA (crR1-2.23^{ANT1}) was also tested with LbCas12a_gRNA2 (Supplemental Figure 4), which was previously used by Vu and coworkers (Vu et al., 2020). Our data collected from 6 biological replicates were processed and compared using uncorrected Fisher's LSD test. The statistical analysis demonstrated very mild changes in GT efficiency among the GT constructs using single crRNAs with both LbCas12a variants (Figure 3b; pHRC11, pHRC12, and pHRC13 for LbCas12a; and pHRC17, pHRC18, and pHRC19 for ttLbCas12a). The ttLbCas12a-based dual crRNA constructs (pHRC20, pHRC21, and pHRC22) showed higher GT efficiencies than LbCas12a (pHRC14, pHRC15 and pHRC16, respectively), although the p-values were only close to 0.05 and significant (Figure 3b). The highest difference in GT efficiency was found between ttLbCas12a-containing pHRC21 ($9.74 \pm 1.49\%$) and LbCas12a-containing pHRC15 ($6.44 \pm 0.75\%$) with crR1-3.20^{ANT1}, exhibiting a 1.51-fold change ($p = 0.07$) (Figure 3b and c).

In parallel with this experiment, we utilized targeted deep sequencing to analyze the cleavage activity of the nucleases with each of the gRNAs (Figure 3c) at 10 dpt. Due to the large size (~0.3x0.3 cm) of the cotyledon explants used in the previous study, the majority of the cells were not in direct contact with the agrobacteria and thus were not all transformed. Therefore, we reduced the size of the cotyledon explant to ~0.1x0.3 cm (Supplemental Figure 8) to reduce the untransformed cell portion for assessing the editing efficiency by targeted deep sequencing. The data collected from two biological replicates showed

strong enhancement of indel mutation efficiencies of a gRNA if it was used in a dual crRNA construct, regardless of the LbCas12a variants. The largest enhancement was from LbCas12a_gRNA1 (23 nt) in the single crRNA crR1.23^{ANT1}-carrying pHR11 (0.05%) and the dual crRNA crR1-3.23^{ANT1}-expressing pHRC16 (1.66%) in replicate 1, representing a 33.2-fold increase (Figure 3c). The cleavage activity of ttLbCas12a was also higher than that of the WT variant when single cuts were used. For example, in the case of the crR1.23^{ANT1}-expressing constructs, the indel mutation efficiency was 5.00- to 7.29-fold increased with ttLbCas12a (pHRC17) compared to LbCas12a (pHRC11) (Figure 3c). For the cases of the dual crRNAs, ttLbCas12a showed more balanced indel mutation efficiencies between the two gRNAs used in the same construct, especially when the dual crRNA crR1-3.20^{ANT1} with 20-nt gRNAs was examined (Figure 3c, pHRC21, and pHRC22 compared to pHRC15, and pHRC16, respectively). This activity might be one of the reasons that better enhancement of GT efficiency was mediated by ttLbCas12a compared to the WT version.

ttLbCas12a shows better performance than WT LbCas12a in allele-associated marker-free GT at the SIHKT1;2 and SIEPSPS1 loci

To further validate and utilize ttLbCas12a in our research on GT, we compared its performance at the two loci without using any donor-associated selection marker, and no allele-associated selection was employed during the experiments. The salt-tolerant allele SIHKT1;2 (N217D) (Figure 4a) was successfully edited using our LbCas12a-based GT system (Vu et al., 2020), although at low efficiency. We introduced two glyphosate-resistant alleles of tomato 5-enolpyruvylshikimate-3-phosphate synthase 1 (SIEPSPS1): (1) T178I and P182S (TIPS allele, corresponding to T103I and P107S in maize, patent no. US6566587B1) (Lebrun, 2003) (Figure 4b) and (2) G177A and A268T (GAAT allele, corresponding to G102A and A193T in maize, patent no. US 6225114 B1) (Eichholtz, 2001) (Supplemental Figure 9). Extensive comparisons of GT efficiency between LbCas12a and ttLbCas12a were conducted with single crRNAs (crR1.20^{HKT1;2} and crR2.20^{HKT1;2}) and dual crRNAs (crR1-2.20^{HKT1;2} and crR1-2.23^{HKT1;2}) (Figure 4a; Supplemental Figure 10 and Data S1 file) at the SIHKT1;2 locus. A T-DNA-based GT construct was also used in parallel with the replicon-based construct and the dual crR1-2.20^{HKT1;2} construct. Additional comparisons were performed with the dual crRNAs crR1-2.23^{EPSPS1} and crR1-3.23^{EPSPS1} (Figure 4b; Supplemental Figure 10 and Data S1 file) to replace the TIPS and GAAT alleles, respectively, at the SIEPSPS1 locus.

GT efficiency calculated by GT deep sequencing reads only showed precise gene editing at both loci in cases of dual crRNAs, although at low efficiencies (Figure 4c). No GT read was obtained from the replicon-based single crRNA constructs and the T-DNA-based dual crRNA regardless of the LbCas12a variants. At the SIHKT1;2 locus, the GT efficiency was higher for ttLbCas12a using the dual 20-nt crRNA (crR1-2.20^{HKT1;2}), but contrasting results were obtained with the longer dual crRNA (crR1-2.23^{HKT1;2}) (Figure 4c). However, we obtained higher GT efficiency with the 23-nt dual crRNA (crR1-2.23^{EPSPS1}) for the replacement of the TIPS allele using ttLbCas12a (Figure 4c). These data indicate that the targeted deep

sequencing method may help to identify the GT reads among the constructs, although the read numbers were still too low to be used for statistical comparisons. The indel mutation efficiency obtained from the T-DNA construct was up to 15-fold lower than that of the replicon using the same crR1-2.20^{HKT1;2} (Figure 4c). In this experiment, the indel mutation efficiencies of the single crRNAs were also lower than those of the dual crRNAs. The highest indel mutation activity was obtained with crR1-2.20^{HKT1;2} and LbCas12a, yielding values of 4.32% of LbCas12a_gRNA1 and 2.56% of LbCas12a_gRNA2. The gap between the indel mutation efficiencies of LbCas12a_gRNA1 and LbCas12a_gRNA2 from crR1-2.20^{HKT1;2} was also lower in the case of ttLbCas12a. However, ttLbCas12a did not perform well when it was expressed with the 23-nt dual crRNA (crR1-2.23^{HKT1;2}); hence, no GT read was obtained at 10 dpt using the combination (Figure 4c). In general, between the two replicates, higher indel activity in a construct was correlated with higher GT efficiency.

Additional experiments for the exchange of the GAAT allele using the 23-nt dual crRNAs with two (crR1-3.23^{EPSPS1}) or four cleavage sites (crR1-2.23^{EPSPS1} and crR2-4.23^{EPSPS1}) and the LbCas12a variants (Supplemental Figs. 9-10) demonstrated that ttLbCas12a performed better in either case. In triplicate, the highest GT efficiency was obtained with ttLbCas12a-expressing constructs (pHRES2.11 compared to pHRES2.9) using the dual crRNA crR1-3.23^{EPSPS1}, up to $0.015 \pm 0.015\%$ for G177A and $0.018 \pm 0.009\%$ for A268T (Figure 5a). Notably, the four crRNA constructs (pHRES2.10 and pHRES2.12) showed a mild reduction in the gRNA1 and gRNA3 indel mutation efficiencies, which were expected to be higher than those of the dual gRNA-expressing constructs due to the synergistic effects of two close cleavage sites (Figure 5a).

To further validate the performance of the LbCas12a variants, we screened and analyzed transformants obtained from the transformation of the LbCas12a- and ttLbCas12a-based constructs for the exchange of the TIPS allele. CAPS screening by Bpil digestion of the PCR products flanking SIEPSPS1-targeted site 1 demonstrated potential TIPS allele-carrying events (Figure 5b). The Bpil site located 84 bp downstream of the T178 codon was modified during the cloning of the homologous DNA donor through the Golden gate cloning method. Therefore, the undigested bands that appeared on the agarose gel were potentially derived from the TIPS-carrying alleles. Using the PCR products of the events that showed undigested bands in the CAPS assay for targeted deep sequencing analysis revealed several transformants carrying the precise GT allele at various frequencies and up to 9.003% in the case of the H281.82 plant generated with the ttLbCas12a construct (Table 1). Interestingly, the GT frequency revealed from ICE Synthego decomposition of the Sanger data of the same event showed only at 7% (Supplemental Figure 11). Two of the transformants (#H281.50 and #H281.82) obtained by the ttLbCas12a-based construct show targeted deep sequencing GT frequency at more than 5% that may be potential for obtaining inherited offsprings (Table 1). Based on that threshold frequency, we revealed that only the ttLbCas12a construct resulted in 2.78% GT efficiency at the plant stage (Figure 5c). Besides, Sanger sequencing of the purified PCR products from 77 and 72 transformants of the wt LbCas12a and ttLbCas12a variant, respectively, and analysis of their .ab1 files by ICE Synthego (Hsiao et al., 2019) identified similar indel mutation efficiencies induced by the Cas proteins (Figure 5d). The average indel mutation efficiency was $29.36 \pm$

2.84% with LbCas12a and a similar rates for ttLbCas12a ($28.03 \pm 3.24\%$) ($p = 0.5389$, Student's t-test). Notably, the SIEPSPS1 TIPS allele-carrying GT plants showed no phenotypic changes compared to the WT plant (Supplemental Figure 12, pHRES2.8 events #82). Several events that contained high indel mutation rates exhibited phenotypic defects compared to WT (Supplemental Figure 12, pHRES2.7 events #27 and 28).

NU7441 treatment enhances the ttLbCas12a-base GT in tomato

Previously, NU7441 exhibited enhancement of LbCas12a-based GT with SIANT1 as a visible marker (Figure 1b). To further optimize ttLbCas12a-based GT in tomato, we investigated the impacts of various NU7441 concentrations on the GT process using ttLbCas12a constructs with crR1-2.20^{HKT12}. Targeted deep sequencing data demonstrated the enhancement of GT efficiency with 1 μ M NU7441 added to the culture medium albeit at low read numbers. However, when the NU7441 concentrations were higher, the GT efficiency was lower than that of the mock control (Figure 5e). Notably, the NU7441 treatments at various concentrations showed only mild changes in the indel mutation efficiency of gRNA1 and gRNA2 of the dual crRNA (Figure 5e).

Discussion

The introduction of DNA DSB(s) at the targeted sites was shown to dramatically enhance GT efficiency in plants (Puchta et al., 1996). DSB repair is dictated by the NHEJ mechanism due to the abundance of KU70/80 and the other components in the cells (Van Vu et al., 2019). Therefore, the plant HDR efficiency is considerably lower than that of NHEJ. The HDR pathway is more strictly dependent on the cell cycle, and even during favorable S-G2 phases, HDR must also compete with NHEJ to repair DNA DSBs. Previously, accumulated data in animal and plant studies showed the possibility of regulating repair pathway determination or inhibiting cNHEJ components by biochemical or chemical approaches (Chu et al., 2015; Endo et al., 2016; Maruyama et al., 2015; Nishizawa-Yokoi et al., 2016; Robert et al., 2015; Song et al., 2016; Srivastava et al., 2012; Zhang et al., 2017). Among the chemicals that exhibited positive effects on HDR or GT in animals, we chose to study several chemicals that inhibit the cNHEJ component(s) to enhance GT efficiency in tomato.

DNA ligase IV was shown to be involved in the last step of cNHEJ-mediated DSB repair to seal the broken ends of DNA DSBs. In a cell-free system, human DNA ligase IV was inhibited by SCR7, a small molecule chemical, by blocking its DNA binding activity (Srivastava et al., 2012). SCR7 at a concentration of 1 μ M was shown to enhance CRISPR/Cas9-based GT efficiency up to 5-fold (Chu et al., 2015) or 19-fold (Maruyama et al., 2015) in mammalian and mouse cells, and 10 μ M or 60 μ M SCR7 treatment led to reduced transfection efficiency and cell viability. However, our data demonstrate only a moderate increase in GT efficiency with the SpCas9 construct at toxic levels of SCR7 in animals and no significant enhancement of GT efficiency in the case of LbCas12a (Figure 1a; Supplemental Table 1). Because DNA

ligase IV inhibition by SCR7 was irrespective of the DSB configuration (Srivastava et al., 2012), the DNA DSBs generated by either SpCas9 or LbCas12a were not expected to affect the inhibition strength. Since our improved LbCas12a-based GT system showed high efficiency under the experimental conditions, the addition of SCR7, which affects the final step of cNHEJ, may not be recognized easily, and the impacts of its toxicity level may be more visible (Figure 1a). There were limited data regarding the uses of SCR7 for CRISPR/Cas-based GT enhancement in plants; therefore, it is unclear if the SCR7 treatment is species-dependent, since the uptake of SCR7 may be different in plants. The enhancement impacts of SCR7 were also controversial in animals since studies that used human cell lines or rabbit embryos did not show significant improvement of CRISPR/Cas9- or TALEN-based GT efficiency by SCR7 (Gutschner et al., 2016; Song et al., 2016; Yang et al., 2016).

One of the alternative strategies for blocking the cNHEJ pathway is to inhibit the DNA-PKcs or the other DNA-dependent protein kinases of the PI-3K family by NU7441 (Leahy et al., 2004) or KU0060648 (Munck et al., 2012). Studies conducted on mammalian cells showed that CRISPR/Cas9-based GT efficiency is enhanced up to twofold by using NU7441 or KU0060648 (Robert et al., 2015). However, treatment with 1 μ M NU7441 and 200 nM KU0060648 did not significantly enhance the SpCas9-based GT efficiency under our experimental conditions, although only NU7441 significantly enhanced the LbCas12a-based GT efficiency up to 1.51-fold in the case of the multireplicon construct (Figure 1b; Supplemental Table 2) thanks to its ability to supply the homologous donor templates by the smaller-sized replicons (Vu et al., 2020). The NU7441 treated sample transformed with the LbCas12a-based single replicon pHR01 showed a tendency of higher GT efficiency compared to the control with the p-value was closed to 0.05. Since no plant homologs of DNA-PKcs have been identified, these data were surprising but were within our expectations for the existence of other types of plant DNA-dependent protein kinases (Van Vu et al., 2019). More importantly, these data indicate that the inhibitory effects of NU7441 and KU0060648 were selective for the kinase forms and the configurations of DNA DSB ends. Notably, although KU0060648 showed a wider range of inhibition of both DNA-PKcs and PI-3K compared to NU7441, only NU7441 had a positive impact on the LbCas12a GT tools, indicating that the kinase targets of KU0060648 and NU7441 in tomato were distinct.

To further improve GT systems, recent studies using polyamines (Lee et al., 2019) and silver nitrate, a polyamine biosynthesis regulator, were conducted. In a cell-free assay, polyamines were shown to facilitate RAD51 activities during the formation of synaptic complexes and strand invasion. Depletion of polyamines resulted in the impairment of HDR in mouse hair follicle cells. However, to the best of our knowledge, no direct evidence of the addition of polyamines exerting stimulatory effects on HDR has been reported. Although direct supplementation with polyamines did not affect the CRISPR/Cas-based GT efficiency under our experimental conditions, when we treated the explants with silver nitrate, indirect stimulation of polyamine production using silver nitrate increased GT events, which appeared as purple counting data at 21 dpt (Supplemental Figure 3a). In the regeneration stage, silver nitrate might also suppress the activities of ethylene released under the stress induced by agrobacteria and tissue culture processes, leading to the promotion of embryogenic callus proliferation and subsequent shoot regeneration (Supplemental Figure 3b) (Beyer, 1976; Giridhar et al., 2004; Roustan et al., 1990).

Previously, we showed that our LbCas12a-based GT system-mediated GT more effectively than did SpCas9 complexes (Vu et al., 2020). However, direct evidence for the comparison is still required, considering that the accessibility of the cleavage sites and loci by CRISPR/Cas complexes may exhibit different results. Therefore, in this study, we selected the well-characterized SIANT1 locus and its two cleavage sites (1 and 3) to compare the two nucleases using the same or very closed gRNA binding sites (Figure 2a and Supplemental Figure 4). The only difference between the SpCas9- and LbCas12a-based vectors was the coding sequence of each of the nucleases, and they were both human-codon optimized (Figure 2b and Supplemental Data S1 file). As expected, the LbCas12-based GT tools outperformed the SpCas9-based replicons at the same cleavage sites (Figure 2c). Notably, assessment of indel mutation efficiencies of the two systems at the plant stage demonstrated a reverse correlation with the GT efficiencies, as the SpCas9-based indel mutation efficiencies were significantly higher than those of the LbCas12a complexes at the tested cleavage sites (Figure 2d and Supplemental Figure 5). We reason that the strong cleavage activities of the SpCas9 complexes at all the cell cycles may lead to inhibition of the cleavage sites for further recurrent cuts and hence a reduction in the probability of homologous DNA donor-mediated repair by GT in the S-G2 HDR favorable phases. Another important point is that LbCas12a cleaves the targeted sites at a distal side of the TTTV PAM; hence, recurrent cleavages may be possible if the DSB repair of the first cut did not affect the seed sequence located at the proximal side of the PAM (Vu et al., 2020). The view was also supported by a recent study (Huang et al., 2021). We cannot exclude the possibility that the difference in the DNA DSB configurations of SpCas9 (mostly blunt ends) and LbCas12a (cohesive ends) differentially determined repair pathway activation in a spatiotemporal manner, which resulted in the difference in GT efficacy of the two nucleases. In addition, this experiment also indicates that the T-DNA-based gene editing efficiencies were notably low compared to that of the replicon system (Figure 2c, d) at the same cleavage sites due to its low copy nature.

Recently, in attempts to further improve GT efficiency in plants, Puchta's group found that a single mutation (D156R) of LbCas12a significantly improved GT performance compared to WT nuclease (Huang et al., 2021; Merker et al., 2020b), especially at the optimal temperature for plant growth. However, a direct comparison of the LbCas12a variants in somatic cell systems has not been reported. Our data not only provide a direct comparison of the two nucleases but also showed their crRNA preference (Figure 3) in tomato somatic cells for practical applications. There was no significant improvement in GT efficiency using single crRNAs, but we observed that the ttLbCas12a-based GT might be enhanced with the dual crRNAs although the p-value was not less than 0.05 ($p=0.0714$), especially with the 20-nt crRNAs at the SIANT1 locus (Figure 3c). The weak improvement in GT efficiency mediated by ttLbCas12a compared to the data published by Puchta's group (Huang et al., 2021; Merker et al., 2020a) could be explained by the high-temperature experimental conditions applied from day 3 to day 12 throughout our study (Supplemental Figure 1), which might reduce the low-temperature tolerance advantages of ttLbCas12a. The slight difference from the 20-nt crRNAs might also be explained by the potential *trans* activities of the LbCas12a-crRNA complexes without affecting the on-target activities (Figure 3c) (Fuchs et al., 2019). Further comparison of the LbCas12a variants at the other two loci, SIHKT1;2 and SIEPS1, without using a donor or GT allele-associated selection marker showed better performance of ttLbCas12a

with dual 20-nt crRNAs at SIHKT12a (Figure 4) and dual 23-nt crRNAs at SIEPSPS1 loci (crR1-2.23^{EPSPS1} and crRNA1-3.23^{EPSPS1}) (Figures 4 and 5a). The data demonstrated the importance of using two neighboring (Figure 4a and b) or distancing cleavages (Supplemental Figure 9) for efficient GT, as this approach might offer synergistic effects in the case of neighboring cleavages that lead to considerably higher cutting (Chen et al., 2017). In the case of GT alleles that require two distanced sequence modifications, such as the GAAT allele of the SIEPSPS1 loci, two DSBs flanking the targeted sites may ensure simultaneous exchanges of the sequences, since the HDR-based conversion tract generated from each targeted site may not cover the other, due to length limitations (Huang et al., 2021).

Analysis of the transformants obtained from the GT experiment for exchanging the TIPS allele of SIEPSPS1 without using an allele-associated selection marker (i.e. glyphosate herbicide) revealed high GT efficiency (2.78 %) at the plant stage only with the ttLbCas12a-based construct (Figure 5c, Table 1). The number of analyzed plants might not be sufficiently high to obtain transformants with more than 5 % GT frequency in the case of the LbCas12a-based construct. The transformants carrying up to 9.003 % of the GT allele (Table 1) were found with normal phenotypes compared to WT parental plants (Supplemental Figure 12). Nonetheless, it would be important to evaluate the inheritance of the GT allele in the next generations, which was also shown in our previous report with the SIHKT1;2 N217D GT allele using the similar replicon-LbCas12a combination (Vu et al., 2020). We also observed abnormal phenotypes of the transformants carrying high indel mutation rates, especially those obtained from the LbCas12a-based construct. It was due to the high rates of SIEPSPS1 indel mutation alleles present in the same event. The malfunction of the SIEPSPS1 protein might lead to the inefficiency of aromatic amino acid biosynthesis, which causes phenotypic defects. Finally, we confirmed the stimulating impacts of 1 μ M NU7441 on ttLbCas12a-based GT performance. However, due to the limited number of the targeted deep sequencing reads that carried the GT allele, even with the thin cotyledon explants, the potentially positive roles of NU7441 in plant GT may be further confirmed by targeted deep sequencing using a protoplast system. Considering that only the ttLbCas12a resulted in events carrying moderate TIPS GT frequencies among fewer than a hundred analyzed plants without using any allele-associated selection marker, ttLbCas12a is a better choice for plant GT. Our findings from this work may add more or less positive information for the improvement of the plant GT system and may further facilitate its practical applications for precision crop breeding.

Conclusion

The natural HDR efficiency in plant somatic cells is too low to be utilized for practical applications of GT-mediated plant breeding. Continuous efforts to improve GT performance have been undertaken for precision crop breeding. In this study, we further improved the LbCas12a-based GT system with the use of chemical treatments (1 μ M of NU7441 and/or AgNO₃). The impacts of small molecule chemical treatments on GT have not been well studied in crop plants. Therefore, our data for the assessment of the effects of SCR7, NU7441, and KU0060648 treatments on GT efficiency may help to elucidate their impacts and possible targeted components for HDR pathway regulation in plants.

Our data show that LbCas12a outperformed SpCas9 under the same experimental conditions at the SIANT1 loci. Similar effects of the replicon system for GT are also clearly indicated. Despite the milder stimulatory effects on GT performance under our experimental conditions due to the high-temperature protocol, the results of this study indicate that ttLbCas12a is a better choice for future applications in practical GT in plants. Taken together, the combination of the replicon with ttLbCas12a, double cleavages flanking the modification sequence, and the addition of NU7441 and/or AgNO₃ and appropriate temperature conditions are important parameters for the application of GT in future practical applications in precision plant breeding.

Experimental Procedures

System design for plant GT in tomato

The SIANT1, SIHKT1;2, and SIEPSPS1 loci were used to conduct HDR-based DNA insertion and allele replacement experiments. The chemical treatment experiments used a single replicon (pTC217 and pHR01) and multiple-replicon tool (pMR01) vectors from previous works (Cermak et al., 2015; Vu et al., 2020) to target the SIANT1 gene. The SpCas9 containing the pTC217 vector was ordered from Addgene (Plasmid #70018) (Cermak et al., 2015). Further works used the single replicon system as a vector for the delivery of guide RNA and CRISPR/Cas expression cassettes and GT donor templates in this study (Figure 2a and Supplemental Data S1 file).

For comparison of the SpCas9 and LbCas12a complexes in GT performance, we designed an HDR-mediated insertion of selection markers at the SIANT1 locus that was well studied in our laboratory (Vu et al., 2020). The gRNA binding and cutting sites were selected in a manner that could be used for both SpCas9 (SpCas9_gRNA1 and SpCas9_gRNA2) and LbCas12a (LbCas12a_gRNA1 and LbCas12a_gRNA3) (Figure 2a). We used a single gRNA for each of the GT vectors with either SpCas9 or LbCas12a (Figure 2b). At the cutting site of LbCas12a_gRNA3, two different gRNA lengths (20 and 23 nt) were tested (Figure 2b). All the editing constructs in the experiment were delivered by *Agrobacterium*-mediated transformation of tomato cotyledon explants, and two sets of constructs were cloned: one set with the single geminiviral replicon system (Vu et al., 2020) for the amplification of homologous DNA donors and the other T-DNA set for comparison.

For the assessment and characterization of the activities of ttLbCas12a in GT in comparison with the wild-type version of LbCas12a, similar constructs were designed for targeting the SIANT1 locus with single LbCas12a crRNA expression cassettes. In addition, dual guide RNA expression cassettes combining LbCas12a_gRNA1 (20 and 23 nt) and LbCas12a_gRNA3 (20 and 23 nt) were also used for the GT experiments (Figure 3a and Supplemental Data S1 file).

A similar system for comparison of ttLbCas12a and wtLbCas12a was designed for targeting the SIHKT1;2 and SIEPSPS1 loci (Figure 4a and b). Single and dual cutting sites were used for SIHKT1;2 (Figure 4a and Supplemental Data S1 file). The gRNA lengths (20 and 23 nt) were also evaluated at the

same locus. For SIEPSPS1, only dual gRNAs 23 nt in length were assessed for GT with the LbCas12a variants (Figure 4 b and Supplemental Data S1 file).

In all the GT vectors, the expression of SpCas9 and LbCas12a variants was driven by a long CaMV 35S promoter that contains an intron (Trp1) at the 5'UTR. A copy of AtUBQ10 intron 1 was also inserted in the coding sequence of the LbCas12a variants (Supplemental Data S1 file), which was tested previously for GT experiments by Vu and coworkers (Vu et al., 2020). The crRNA and sgRNA expression cassettes were transcribed with the support of the core sequence of the AtU6 promoter (Nekrasov et al., 2013).

***Agrobacterium*-mediated tomato transformation and chemical treatments**

Agrobacterium-mediated tomato transformation was conducted following our protocol (Supplemental Figure 1) published previously by Vu and coworkers (Vu et al., 2020). For the treatment of chemicals, the chemicals at the tested concentrations were added to the NSEL medium. The 30 μ M of silver nitrate was also added to the first subcultured SEL4C medium at the later stage for stimulating somatic embryogenesis. The total treatment time was 5 days (day 3 to day 8 post transformation (dpt)). For targeted deep sequencing, cotyledon samples were collected at 10 dpt.

Assessment of GT efficiency

For assessment of the GT efficiency at SIANT1, purple spot counting was conducted at 21 dpt, and purple plants were recorded at the hardening stage. The GT efficiency reflected by the purple spot numbers was calculated with normalization to the SIANT1 overexpression tool that was transformed in parallel with the GT tool. Our calculation method normalized the number of cells/calli that was edited (and hence carrying p35S-ANT1 expression cassette) by the HDR tools to the number of cells that were successfully transformed with a T-DNA harboring over-expression cassette of the ANT1 gene driven by p35S in the same experimental conditions. This calculation may reflect more actual HDR frequency regarding the editing at the cell levels. A similar calculation was used and accepted elsewhere (Puchta et al., 1993; Puchta et al., 1996). This calculation method was also explained in our previous report (Vu et al., 2020).

For assessment of the GT efficiency at the SIHKT1;2 and SIEPSPS1 loci, targeted deep sequencing was conducted with thin cotyledon explants collected at 10 dpt. Sanger sequencing was performed to screen and validate GT plants.

Targeted deep sequencing

Genomic DNAs were isolated from the cotyledon explants (30 explants per sample) or mature leaves (three distinct leaflets from three different young leaves per plant per sample) using the CTAB method.

The MiSeq sequencing service (MiniSeq™ System, Illumina, USA) was used. MiSeq samples were prepared in three PCRs according to the manufacturer's guidelines with genomic DNAs as templates for the first PCR. The first and second PCRs used primers listed in Supplemental Table 5, whereas the third PCRs were performed with the manufacturer's primers to assign sample IDs. The first PCR primers were designed for binding to the upstream and downstream sequences from the homologous donor sequence junctions to avoid amplifying the donor DNA sequences. The second PCR primers were designed to amplify 150-180-bp flanking the targeted base changes at the targeted sites. High-fidelity DNA Taq polymerase (Phusion, NEB, USA) was used for PCR. The MiSeq raw data FASTQ files were analyzed by the Cas-Analyzer tool (Park et al., 2016). The indel analysis window was set to 5 bases, with a comparison range covering both read ends. The GT efficiency was assessed using the corresponding donor sequence as the input HDR donor sequence.

Statistical analysis

All comparison experiments were conducted with at least 3 replicates, and data were recorded by purple spot counting, targeted deep sequencing, and plant event screening. Some of the experiments using targeted deep sequencing were conducted in two replicates. The editing data, statistical analysis, and plots were further processed by the MS Excel and GraphPad Prism programs and explained in detail in the legends of figures and/or tables. Pairwise comparison data were tested with Student's t-test with unequal variance and two-tailed parameters. Similar parameters were applied for multiple comparisons using Fisher's LSD test. A difference was considered to be significant when the statistical tests returned a p-value < 0.05.

Declarations

ACKNOWLEDGMENT

We wish to thank Mrs. Ngan Nguyen Thi and Mrs. Jeong Se Jeong for providing valuable technical support to this study. This work was supported by the National Research Foundation of Korea (Grant NRF 2020R111A1A01072130, 2020M3A9I4038352, 2020R1A6A1A03044344) and the Program for New Plant Breeding Techniques (NBT, Grant PJ01478401), Rural Development Administration (RDA), Korea.

COMPETING INTERESTS

The authors declare no competing interests.

CONTRIBUTION

T.V.V. and J.Y.K. conceived and designed the research. T.V.V., D.T.H.D., M.T.T., Y.W.S., and Y.J.S. conducted experiments. T.V.V., D.T.H.D., M.T.T. and J.Y.K. analyzed data. T.V.V. wrote the manuscript. T.V.V. and J.Y.K. finalized the manuscript. All authors read and approved the manuscript.

References

- Beyer, E.M. (1976). A potent inhibitor of ethylene action in plants. *Plant Physiol* *58*, 268-271.
- Butler, N.M., Baltes, N.J., Voytas, D.F., and Douches, D.S. (2016). Geminivirus-Mediated Genome Editing in Potato (*Solanum tuberosum* L.) Using Sequence-Specific Nucleases. *Front Plant Sci* *7*, 1045.
- Cermak, T., Baltes, N.J., Cegan, R., Zhang, Y., and Voytas, D.F. (2015). High-frequency, precise modification of the tomato genome. *Genome Biol* *16*, 232.
- Chen, F., Ding, X., Feng, Y., Seebeck, T., Jiang, Y., and Davis, G.D. (2017). Targeted activation of diverse CRISPR-Cas systems for mammalian genome editing via proximal CRISPR targeting. *Nat Commun* *8*, 14958.
- Chu, V.T., Weber, T., Wefers, B., Wurst, W., Sander, S., Rajewsky, K., and Kuhn, R. (2015). Increasing the efficiency of homology-directed repair for CRISPR-Cas9-induced precise gene editing in mammalian cells. *Nat Biotechnol* *33*, 543-548.
- Eichholtz, D.A., Scott, G.C., Murthy, K.G. (2001). Modified gene encoding glyphosate-tolerant 5-enolpruvyl-3-phosphoshikimate synthase. US Patent no US6,225,114B1.
- Endo, M., Mikami, M., and Toki, S. (2016). Biallelic Gene Targeting in Rice. *Plant Physiol* *170*, 667-677.
- Fuchs, R.T., Curcuru, J., Mabuchi, M., Yourik, P., and Robb, G.B. (2019). Cas12a trans-cleavage can be modulated in vitro and is active on ssDNA, dsDNA, and RNA. 600890.
- Gil-Humanes, J., Wang, Y., Liang, Z., Shan, Q., Ozuna, C.V., Sanchez-Leon, S., Baltes, N.J., Starker, C., Barro, F., Gao, C., *et al.* (2017). High-efficiency gene targeting in hexaploid wheat using DNA replicons and CRISPR/Cas9. *Plant J* *89*, 1251-1262.
- Giridhar, P., Indu, E.P., Vinod, K., Chandrashekar, A., and Ravishankar, G.A. (2004). Direct somatic embryogenesis from *Coffea arabica* L. and *Coffea canephora* P ex Fr. under the influence of ethylene action inhibitor-silver nitrate. *Acta Physiologiae Plantarum* *26*, 299-305.
- Gutschner, T., Haemmerle, M., Genovese, G., Draetta, G.F., and Chin, L. (2016). Post-translational Regulation of Cas9 during G1 Enhances Homology-Directed Repair. *Cell Rep* *14*, 1555-1566.
- Hanfrey, C., Sommer, S., Mayer, M.J., Burtin, D., and Michael, A.J. (2001). Arabidopsis polyamine biosynthesis: absence of ornithine decarboxylase and the mechanism of arginine decarboxylase activity. *Plant J* *27*, 551-560.
- Hsiao, T., Conant, D., Rossi, N., Maures, T., Waite, K., Yang, J., Joshi, S., Kelso, R., Holden, K., Enzmann, B.L., *et al.* (2019). Inference of CRISPR Edits from Sanger Trace Data. 251082.

- Huang, T.-K., Armstrong, B., Schindele, P., and Puchta, H. (2021). Efficient gene targeting in *Nicotiana tabacum* using CRISPR/SaCas9 and temperature tolerant LbCas12a. *Plant Biotechnol J* *doi: <https://doi.org/10.1111/pbi.13546>*.
- Leahy, J.J., Golding, B.T., Griffin, R.J., Hardcastle, I.R., Richardson, C., Rigoreau, L., and Smith, G.C. (2004). Identification of a highly potent and selective DNA-dependent protein kinase (DNA-PK) inhibitor (NU7441) by screening of chromenone libraries. *Bioorg Med Chem Lett* *14*, 6083-6087.
- Lebrun, M., Sailland, A., Freyssinet, G., DeGryse, E. (2003). Mutated 5-enolpyruvylshikimate-3-phosphate synthase, gene coding for said protein and transformed plants containing said gene. US Patent no US6566587B1.
- Lee, C.Y., Su, G.C., Huang, W.Y., Ko, M.Y., Yeh, H.Y., Chang, G.D., Lin, S.J., and Chi, P. (2019). Promotion of homology-directed DNA repair by polyamines. *Nat Commun* *10*, 65.
- Malzahn, A.A., Tang, X., Lee, K., Ren, Q., Sretenovic, S., Zhang, Y., Chen, H., Kang, M., Bao, Y., Zheng, X., *et al.* (2019). Application of CRISPR-Cas12a temperature sensitivity for improved genome editing in rice, maize, and Arabidopsis. *BMC Biol* *17*, 9.
- Maruyama, T., Dougan, S.K., Truttmann, M.C., Bilate, A.M., Ingram, J.R., and Ploegh, H.L. (2015). Increasing the efficiency of precise genome editing with CRISPR-Cas9 by inhibition of nonhomologous end joining. *Nat Biotechnol* *33*, 538-542.
- Merker, L., Schindele, P., Huang, T.K., Wolter, F., and Puchta, H. (2020a). Enhancing in planta gene targeting efficiencies in Arabidopsis using temperature-tolerant CRISPR/LbCas12a. *Plant Biotechnol J* *18*, 2382-2384.
- Merker, L., Schindele, P., and Puchta, H. (2020b). Using CRISPR/ttLbCas12a for in planta Gene Targeting in *A. thaliana*. *Curr Protoc Plant Biol* *5*, e20117.
- Munck, J.M., Batey, M.A., Zhao, Y., Jenkins, H., Richardson, C.J., Cano, C., Tavecchio, M., Barbeau, J., Bardos, J., Cornell, L., *et al.* (2012). Chemosensitization of cancer cells by KU-0060648, a dual inhibitor of DNA-PK and PI-3K. *Mol Cancer Ther* *11*, 1789-1798.
- Nekrasov, V., Staskawicz, B., Weigel, D., Jones, J.D., and Kamoun, S. (2013). Targeted mutagenesis in the model plant *Nicotiana benthamiana* using Cas9 RNA-guided endonuclease. *Nat Biotechnol* *31*, 691-693.
- Nishizawa-Yokoi, A., Cermak, T., Hoshino, T., Sugimoto, K., Saika, H., Mori, A., Osakabe, K., Hamada, M., Katayose, Y., Starker, C., *et al.* (2016). A Defect in DNA Ligase4 Enhances the Frequency of TALEN-Mediated Targeted Mutagenesis in Rice. *Plant Physiol* *170*, 653-666.
- Park, J., Lim, K., Kim, J.-S., and Bae, S. (2016). Cas-analyzer: an online tool for assessing genome editing results using NGS data. *Bioinformatics* *33*, 286-288.

- Paszkowski, J., Baur, M., Bogucki, A., and Potrykus, I. (1988). Gene targeting in plants. *EMBO J* 7, 4021-4026.
- Puchta, H., Dujon, B., and Hohn, B. (1993). Homologous recombination in plant cells is enhanced by in vivo induction of double strand breaks into DNA by a site-specific endonuclease. *Nucleic Acids Research* 21, 5034-5040.
- Puchta, H., Dujon, B., and Hohn, B. (1996). Two different but related mechanisms are used in plants for the repair of genomic double-strand breaks by homologous recombination. 93, 5055-5060.
- Puchta, H., and Hohn, B. (2005). Green light for gene targeting in plants. *Proc Natl Acad Sci U S A* 102, 11961-11962.
- Qi, Y., Zhang, Y., Zhang, F., Baller, J.A., Cleland, S.C., Ryu, Y., Starker, C.G., and Voytas, D.F. (2013). Increasing frequencies of site-specific mutagenesis and gene targeting in Arabidopsis by manipulating DNA repair pathways. *Genome Res* 23, 547-554.
- Robert, F., Barbeau, M., Ethier, S., Dostie, J., and Pelletier, J. (2015). Pharmacological inhibition of DNA-PK stimulates Cas9-mediated genome editing. *Genome Med* 7, 93.
- Roustan, J.-P., Latche, A., and Fallot, J. (1990). Control of carrot somatic embryogenesis by AgNO₃, an inhibitor of ethylene action: Effect on arginine decarboxylase activity. *Plant Science* 67, 89-95.
- Schindele, P., and Puchta, H. (2020). Engineering CRISPR/LbCas12a for highly efficient, temperature-tolerant plant gene editing. *Plant Biotechnol J* 18, 1118-1120.
- Shan, Q., Wang, Y., Li, J., Zhang, Y., Chen, K., Liang, Z., Zhang, K., Liu, J., Xi, J.J., Qiu, J.L., *et al.* (2013). Targeted genome modification of crop plants using a CRISPR-Cas system. *Nat Biotechnol* 31, 686-688.
- Song, J., Yang, D., Xu, J., Zhu, T., Chen, Y.E., and Zhang, J. (2016). RS-1 enhances CRISPR/Cas9- and TALEN-mediated knock-in efficiency. *Nat Commun* 7, 10548.
- Srivastava, M., Nambiar, M., Sharma, S., Karki, S.S., Goldsmith, G., Hegde, M., Kumar, S., Pandey, M., Singh, R.K., Ray, P., *et al.* (2012). An inhibitor of nonhomologous end-joining abrogates double-strand break repair and impedes cancer progression. *Cell* 151, 1474-1487.
- Terada, R., Urawa, H., Inagaki, Y., Tsugane, K., and Iida, S. (2002). Efficient gene targeting by homologous recombination in rice. *Nat Biotechnol* 20, 1030-1034.
- Van Vu, T., Sung, Y.W., Kim, J., Doan, D.T.H., Tran, M.T., and Kim, J.Y. (2019). Challenges and Perspectives in Homology-Directed Gene Targeting in Monocot Plants. *Rice (N Y)* 12, 95.
- Vu, T.V., Sivankalyani, V., Kim, E.J., Doan, D.T.H., Tran, M.T., Kim, J., Sung, Y.W., Park, M., Kang, Y.J., and Kim, J.Y. (2020). Highly efficient homology-directed repair using CRISPR/Cpf1-geminiviral replicon in

tomato. *Plant Biotechnol J*.

Wright, D.A., Townsend, J.A., Winfrey, R.J., Jr., Irwin, P.A., Rajagopal, J., Lonosky, P.M., Hall, B.D., Jondle, M.D., and Voytas, D.F. (2005). High-frequency homologous recombination in plants mediated by zinc-finger nucleases. *Plant J* *44*, 693-705.

Yang, D., Scavuzzo, M.A., Chmielowiec, J., Sharp, R., Bajic, A., and Borowiak, M. (2016). Enrichment of G2/M cell cycle phase in human pluripotent stem cells enhances HDR-mediated gene repair with customizable endonucleases. *Scientific Reports* *6*, 21264.

Zetsche, B., Heidenreich, M., Mohanraju, P., Fedorova, I., Kneppers, J., DeGennaro, E.M., Winblad, N., Choudhury, S.R., Abudayyeh, O.O., Gootenberg, J.S., *et al.* (2017). Multiplex gene editing by CRISPR–Cpf1 using a single crRNA array. *Nature Biotechnology* *35*, 31-34.

Zhang, J.P., Li, X.L., Li, G.H., Chen, W., Arakaki, C., Botimer, G.D., Baylink, D., Zhang, L., Wen, W., Fu, Y.W., *et al.* (2017). Efficient precise knockin with a double cut HDR donor after CRISPR/Cas9-mediated double-stranded DNA cleavage. *Genome Biol* *18*, 35.

Zhang, Y., Zhang, F., Li, X., Baller, J.A., Qi, Y., Starker, C.G., Bogdanove, A.J., and Voytas, D.F. (2013). Transcription activator-like effector nucleases enable efficient plant genome engineering. *Plant Physiol* *161*, 20-27.

Tables

Table 1. GT efficiency revealed from transformants by targeted deep sequencing

No.	Cas12a variant	Transformant*	Total reads	GT frequency (%)	Indel rate gRNA1 (%)
1	LbCas12a	H273-4	22620	0.000	99.832
2		H273-10	22730	0.000	100.000
3		H273-12	27245	0.000	100.000
4		H273-13	20569	0.000	100.000
5		H273-27	21295	0.000	99.915
6		H273-28	27632	0.000	99.913
7		H273-29	28425	0.000	100.000
8		H273-30	24552	0.000	99.935
9		H273-37	18258	0.000	99.173
10		H273-44	17520	0.040	80.525
11		H273-46	21303	0.000	100.00
12		H273-49	20361	0.000	99.72
13		H273-54	24244	0.008	99.59
14		H273-81	24823	0.004	100.00
15	ttLbCas12a	H281-2	24049	0.403	95.04
16		H281-3	25966	0.004	100.00
17		H281-12	25973	0.000	99.97
18		H281-19	26908	0.000	100.00
19		H281-26	21048	0.005	99.98
20		H281-27	2823	0.071	93.02
21		H281-36	28424	0.000	99.96
22		H281-42	21637	0.083	18.27
23		H281-48	25078	0.355	13.10
24		H281-49	27841	0.000	99.99
25		H281-50	26571	6.315	82.83
26		H281-53	25272	0.004	45.28
27		H281-55	22867	0.000	99.44
28		H281-60	24409	0.000	98.06
29		H281.82	96066	9.003	6.642

*samples with undigested bands obtained in the CAPS assays as the potential GT allele-carrying transformants

Figures

Figure 1

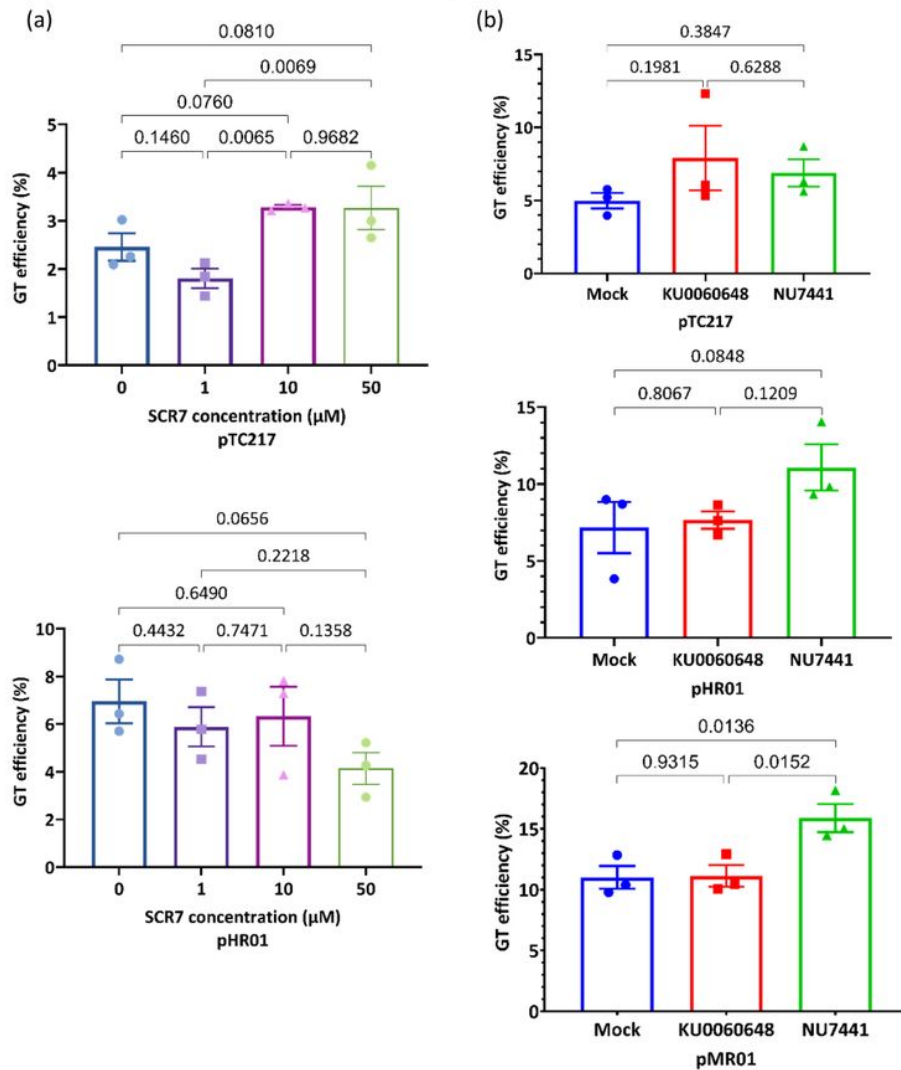


Figure 1

Enhancement of GT efficiency by chemical treatments for blocking cNHEJ. (a) SpCas9 (pTC217, top panel) and LbCas12a (pHR01, bottom panel)-based GT efficiency obtained from the treatment of different SCR7 concentrations. SCR7 was added to the nonselection medium (NSEL), and the explants were incubated for 5 days before transferring to the selection medium (SEL5). The GT efficiencies were calculated at 21 dpt. (b) The impacts of KU0060648 and NU7441 on CRISPR/Cas-based GT. SpCas9-based pTC217 (top panel) and LbCas12a-based pHR01 (middle panel) were cloned with single geminiviral replicons, whereas LbCas12a-based pMR01 (bottom panel) was released from a multireplicon vector. The chemical was added to the nonselection medium (NSEL), and the explants were incubated for 5 days before transferring to the selection medium (SEL5). The GT efficiencies were calculated at 21 dpt. Multiple comparisons of the means and plotting were conducted by GraphPad Prism version 9 using one-way ANOVA and Fisher's LSD test. The p-values of each compared mean pair are shown on the top of the bars.

Figure 2

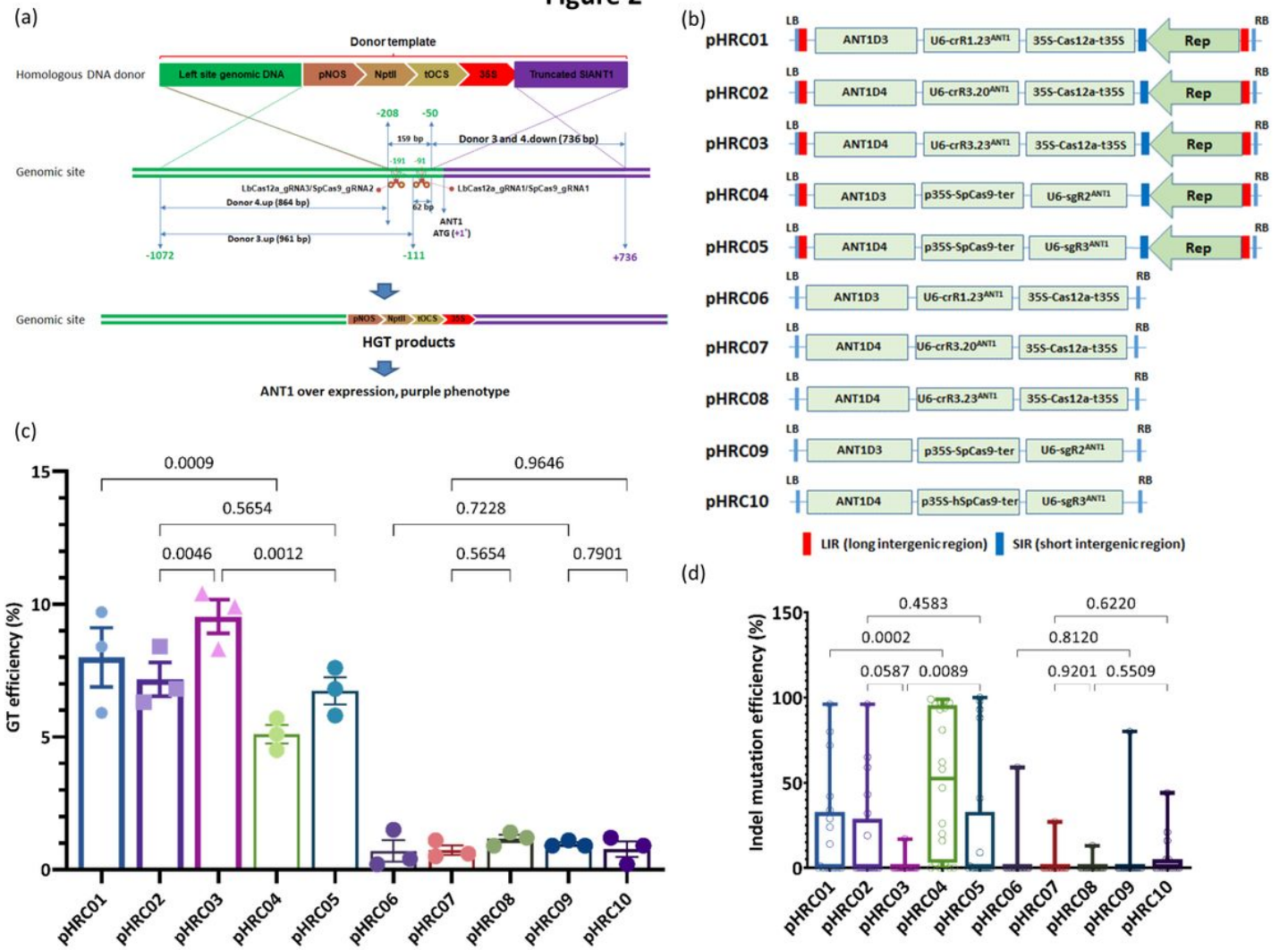


Figure 2

Performance of the LbCas12a and SpCas9 nucleases in GT-mediated DNA insertion in tomato. (a) Schematic diagram of CRISPR/Cas-based GT processes. The SIANT1 genomic site was cleaved by the CRISPR/Cas complexes at the positions of LbCas12a_gRNA1 and 3 and SpCas9_gRNA1 and 2, denoted by scissors. Subsequent repairs of the DSBs were conducted with the addition of donor templates that contain upstream homologous arms (corresponding to Donor 3.up and Donor 4.up) and downstream truncated SIANT1 (corresponding to Donors 3 and 4.down) of the DSB sites and the inserted sequences containing the kanamycin selection marker (pNOS-NptII-tOCS) followed by a CaMV 35S promoter (35S) for constitutively driving SIANT1 expression. The lengths in bp of the homologous arms are also shown. The distances in bp among the cleaved sites and the starts and ends of the donor sequences were calculated and illustrated in relation to the ATG start codon of the SIANT1 gene with the A as the +1 position. The sequence upstream of the SIANT1 start codon is drawn by the green lines, and purple lines are drawn for the downstream part. The crossing discontinuous lines between the homologous DNA donor and genomic site depict the expected homologous recombination for sequence exchanges. Successful GT would integrate the selection marker and 35S promoter at the DSB sites, thereby

supporting event selection and screening by kanamycin antibiotic and purple phenotype. (b) Binary vectors used for comparison of SpCas9- and LbCas12a-based GT performance. Each vector contained a homologous donor described in (a) and the Supplemental data file Data S1, an expression cassette of sgRNA/crRNA and SpCas9 or LbCas12a expression cassette. Two sets of vectors were used: only T-DNA and replicon-based systems for comparison. (c) Scatter dot-bar plots showing the GT efficiencies of the tested constructs. (d) Boxplot showing the indel mutation efficiencies of the GT constructs at the plant stage. The GT efficiencies were calculated at 21 dpt. Multiple comparisons of the means and plotting were conducted by GraphPad Prism version 9 using one-way ANOVA and Fisher's LSD test. The p-values of each compared mean pair are shown on the top of the bars.

Figure 3

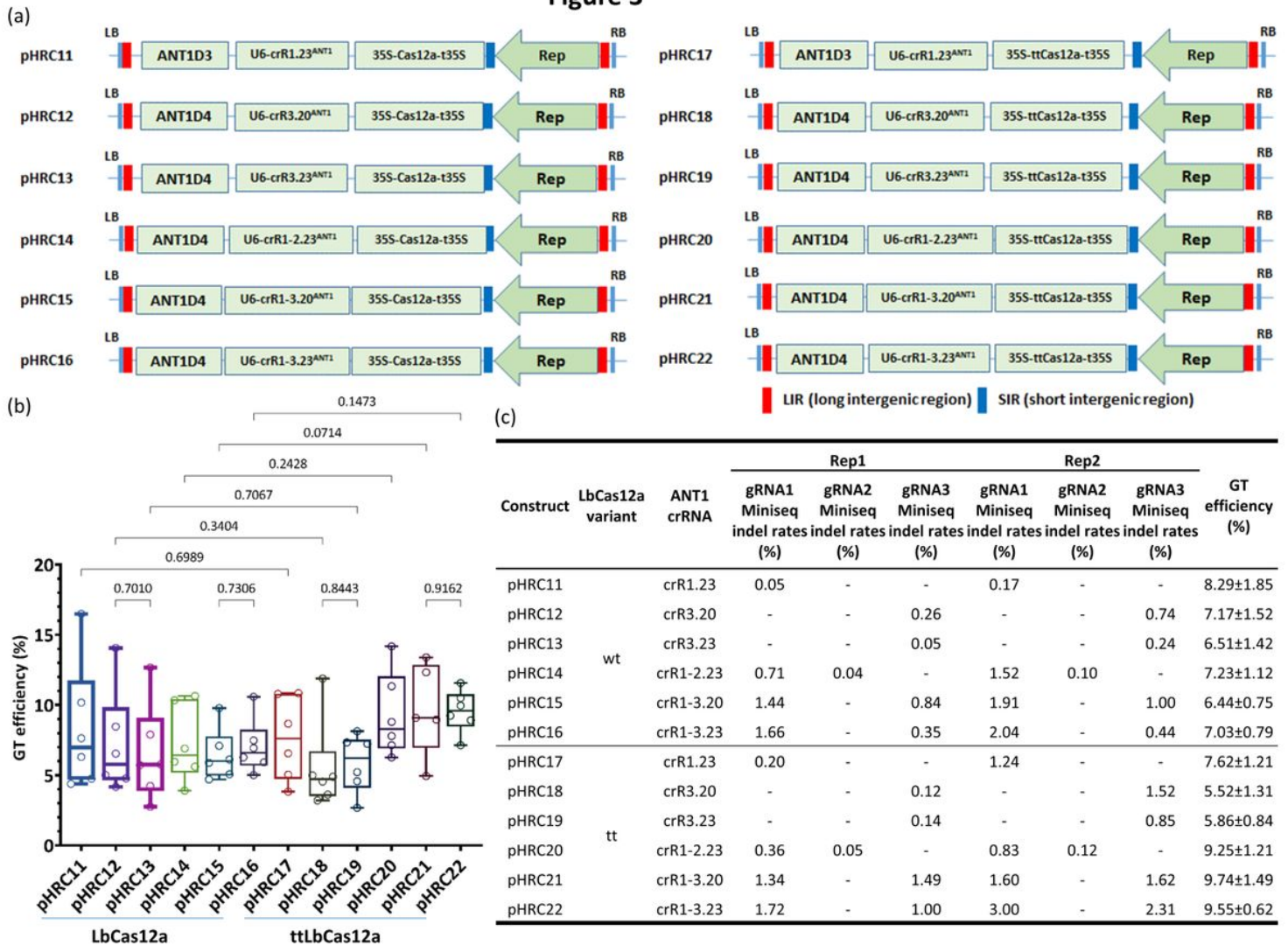


Figure 3

Comparison of GT efficiency between LbCas12a and ttLbCas12a at the SIANT1 locus. (a) Binary constructs with the same crRNAs and donors for the assessment of the GT efficiency of LbCas12a (left panel) and ttLbCas12a (right panel). (b) Boxplot showing the distributions of GT efficiency among the tools using various crRNAs with LbCas12a and ttLbCas12a. Multiple comparisons of the means of GT efficiency of the constructs using the same sets of crRNAs and donors but with LbCas12a or ttLbCas12a

were conducted using Fisher's LSD test, and the p-values are shown above the compared boxes. (c) Indel mutation rates induced by the Cas-crRNA complexes that were assessed at 10 dpt by targeted deep sequencing method. The GT efficiencies are also added for comparison.

Figure 4

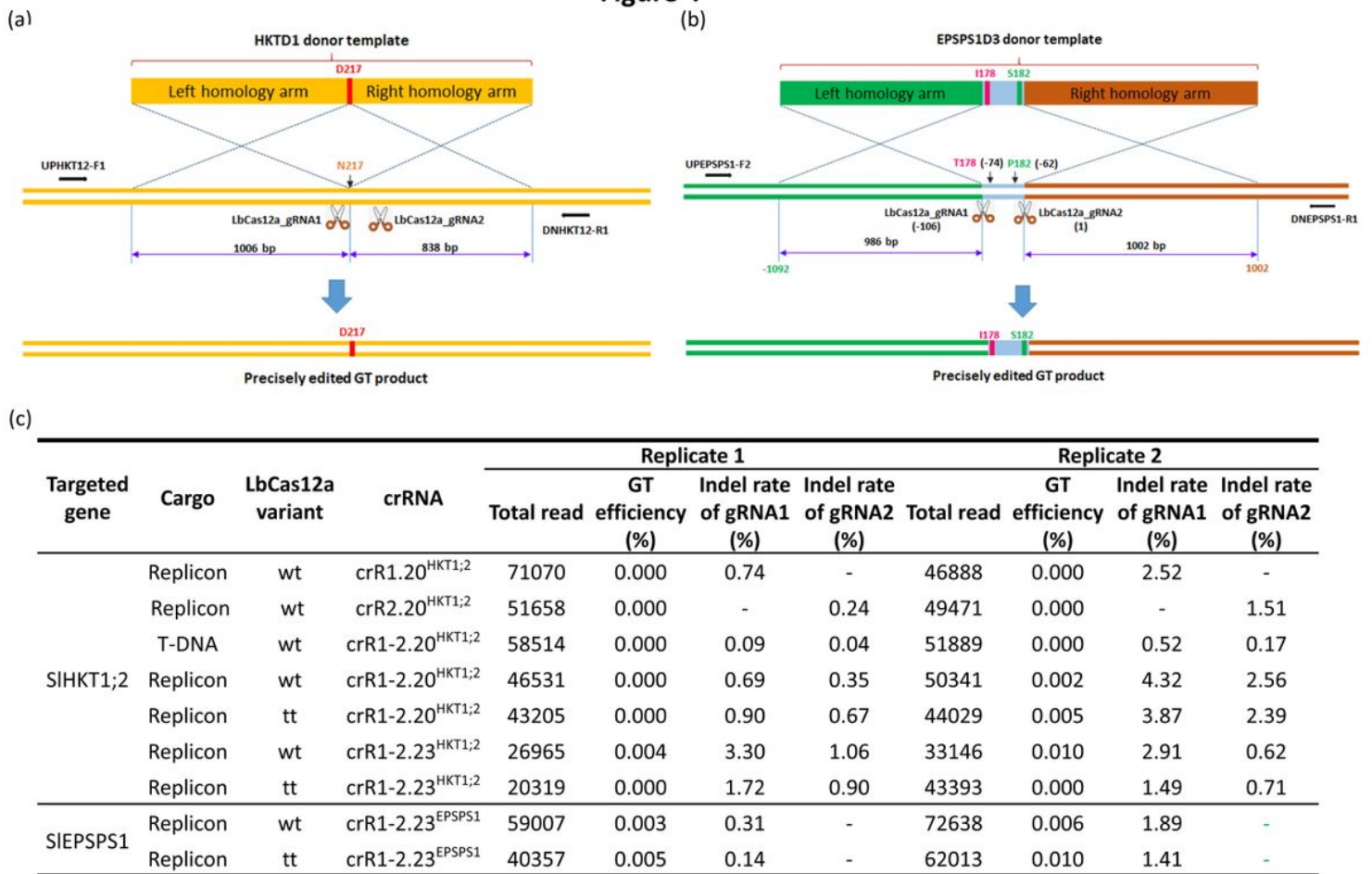


Figure 4

GT performance of the LbCas12a variants at the SIHKT1;2 and SIEPSPS1 loci. (a-b) Schematic diagrams describing the expected GT processes for exchanging the homologous DNA donor template with the genomic sequence at the SIHKT1;2 (a) and SIEPSPS1 (b) loci. The D217 coding sequence was added during the cloning of the HKT1 donor for exchange with the N217 sequence of the genomic site. The lengths of homologous arms are shown. Two cutting sites (LbCas12a cutting sites 1 and 2) were planned to support the GT. The reverse and forward primers for amplifying the targeted sites by PCR are shown with black arrows. The I178 and S182 coding sequences were added during the cloning of the EPSPS1D3 donor for exchange with the T178 and P182 sequences of the genomic site. The lengths of homologous arms are shown. Two cutting sites (LbCas12a cutting sites 1 and 2) were used for the GT experiments. The reverse and forward primers for amplifying the targeted sites by PCR are shown with black arrows. In (b), LbCas12a cutting site 2 is set as position 1, and the other positions are calculated accordingly. The

diagrams were drawn not to their actual scales. (c) The GT and indel mutation efficiencies were assessed by targeted deep sequencing. At the SIHKT1;2 locus, four different crRNAs (single crRNAs: crR1.20HKT12; crR2.20HKT12, and dual crRNAs: crR1-2.20HKT12; crR1.23HKT12) were used for comparison of the LbCas12a variants in GT performance. A T-DNA vector was also used for comparison with the replicon system. With the SIEPSPS1 gene, only one dual crRNA construct (crR1-2.23EPSPS1) was used with the two LbCas12a variants. Wt: wild-type LbCas12a; tt: ttLbCas12a.

Figure 5

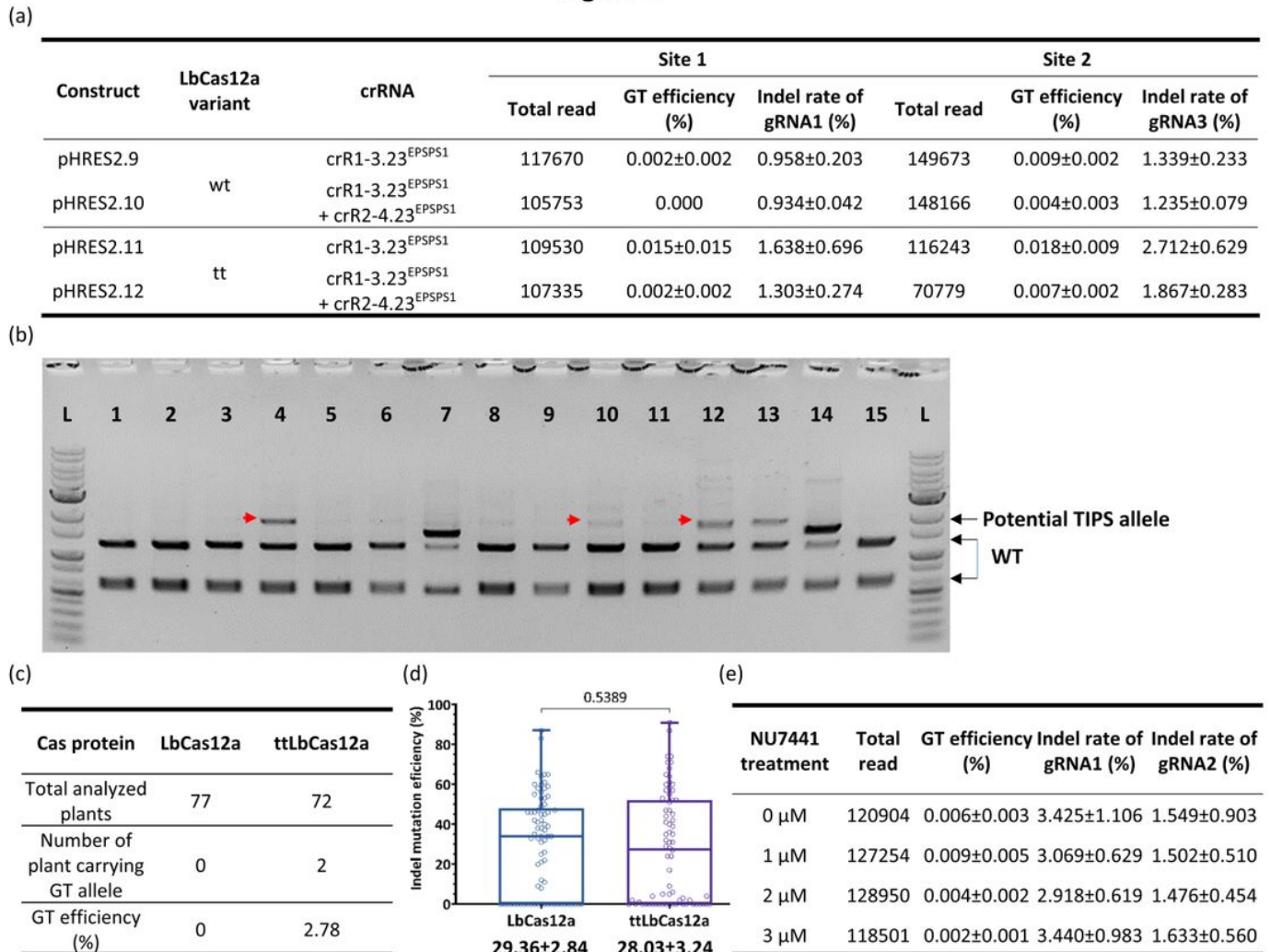


Figure 5

Further assessment of GT performance of the LbCas12a variants at the SIEPSPS1 locus. (a) Assessment of GT efficiency by targeted deep sequencing with GT tools using two or four cutting sites with LbCas12a variants at the SIEPSPS1 locus. (b) Screening of potential GT events using the CAPS assay at the plant stage. Transformants of each LbCas12a variant were obtained from the transformation of the GT tool with the crR1-2.23EPSPS1 expression cassette and used for genomic DNA isolation and PCR amplification of the targeted site with the UPEPSPS1-F2 and DNEPSPS1-R1 primers. The PCR products were purified and digested by the Bpil restriction enzyme since the Bpil site near the targeted site was modified in the DNA donor sequence. The red arrows indicate potential GT bands. 1-15: Representative

transformants obtained from the transformation using the GT construct containing LbCas12a and crR1-3.23EPSPS1. (c) TIPS GT efficiencies obtained with the wt LbCas12a and ttLbCas12a. All the purified PCR products of the transformants that showed undigested bands at WT band size (2314 bp) in the CAPS assay were analyzed by targeted deep sequencing. Only the transformants carrying more than 5% of the TIPS allele were counted as GT events. (d) Boxplots showing indel mutation efficiency induced by LbCas12a and ttLbCas12a. All the purified PCR products used in the CAPS assay were sequenced by the Sanger method, and the ab1 files were subsequently analyzed by ICE Synthego software to reveal the indel mutation and GT efficiencies. The indel mutation efficiencies of all the samples were statistically analyzed using Student's t-test (unpaired, two-tailed, uncorrected) and plotted by GraphPad Prism version 9. The editing efficiencies (mean \pm SEM) are shown at the bottom of each box. (e) Targeted deep sequencing-mediated evaluation of NU7441 impacts on ttLbCas12a-based GT efficiency.

Supplementary Files

This is a list of supplementary files associated with this preprint. Click to download.

- [21.04.26DataS1Sequencesusedinthestudytvv4.docx](#)
- [21.04.26SupplementalfiguresandTablestv4.docx](#)